Twisted Electromagnetic Multi-Gaussian Schell-Model Pulsed Source and Its Propagation

Yan Li and Ming Gao [ORCID]

Abstract—Here, a novel family of random electromagnetic sources (twisted electromagnetic multi-Gaussian Schell-model pulsed beams) exhibiting transverse orbital angular momentum is proposed. The physically realizable conditions for these sources are established, and the analytical formulas of the cross-spectral density matrix elements of the beam propagating through an ABCD optical system are derived within the framework of the extended Collins formula. The behaviors of the spectral density, and the spectral degree of coherence of the beam during transmission are investigated numerically. This work enriches the classical theory of stochastic electromagnetic beams propagation, and may benefit applications requiring a specified degree of beam coherence with transverse orbital angular momentum.

Index Terms—Multi-Gaussian function, optical propagation, optical pulse, transverse orbital angular momentum.

I. INTRODUCTION

FOR nearly 30 years, vortex beams exhibiting orbital angular momentum (OAM) have attracted enormous attention owing to their various potential applications in free-space optical communications (FSOC), optical tweezers, astronomy [1]–[5], etc. In a 1993 paper, Simon and Mukunda introduced the twisted Gaussian Shell-model (GSM) beam [6] exhibiting OAM. This phase, which can only exist in the partially coherent field, can twist the beam around its axis during propagation [6], [7]. Ever since, twisted partially coherent field has generated significant interest. For example, Borghi *et al.* presented a twisted Schell-model beam exhibiting axial symmetry [8]. Mei and Korotkova constructed two different random sources bearing the twisted phase via the modal representation technique [9]. Gori and Santarsiero presented a mathematical method for generating genuine twisted sources [10]. Moreover, unique twisted partially coherent sources, such as twisted electromagnetic beams with structured correlations [11], twisted Laguerre–GSM beams [12], twisted GSM array beams [13], [14], and twisted multi-GSM (MGSM) beams [15], were also introduced successively.

Thus far, most studies on OAM beams have considered the case in which the optical vortices or twisted phase in the wavefronts are along the *x–y* plane, perpendicular to the propagation direction, the *z*-axis [7]. Notably, these beams exhibit longitudinal OAM [7], [16]. Thus, the production of optical fields exhibiting transverse OAM has gained enormous interest. The concepts of twisted space-time (or space-frequency) beams and spatiotemporal optical vortices (STOVs), which exhibit transverse OAM, have been recently introduced [7], [16]–[21]. These findings can avail novel applications in FSOC, optical manipulation, optical tweezers, and other fields.

Conversely, the classical random electromagnetic beams, i.e., electromagnetic Gaussian Schell-Model (EGSM) has been extended to other models exhibiting a special correlation structure, e.g., EMGSM [22], [23], electromagnetic non-uniformly correlated beams [24]–[26], electromagnetic cosine-GSM (EM-CGSM) [27], and electromagnetic Laguerre–GSM sources [28], [29]. These sources exhibit several peculiar properties during transmission because of their special correlation structure. With a few exceptions [26], the previous studies on random electromagnetic beams exhibiting special correlation structures have been limited to stationary conditions.

Non-stationary light fields, such as stochastic optical pulses, are partially spectrally coherent or temporally coherent [30]. Since the concept of the GSM pulsed (GSMP) source was introduced by Paakkonen *et al.* [31], its generation and propagation have been studied extensively [32]–[37].

In this study, we combined the twisted space-frequency beams and random electromagnetic pulsed sources with a multi-Gaussian correlation structure to generate a twisted electromagnetic pulsed fields. These sources exhibit a transverse OAM and rotate along the *x–ω* plane. In Section II, the physically realizable conditions for such beams are established. In Section III, the analytical expressions of the cross-spectral density matrix (CSDM) elements of the beam during propagation are derived based on the extended Collins formula. In Section IV, the simulation results, including other interesting results, are presented and discussed.

Yan Li is with the School of Optoelectronic Engineering, Xi'an Technological University, Xi'an 710021, China (e-mail: liyan2013angel@163.com).

Ming Gao is with the School of Optoelectronic Engineering, Xi'an Technological University, Xi'an 710021, China (e-mail: minggao1964xatu@163.com).

II. THEORETICAL MODEL OF THE TWISTED EMGSMP SOURCES

In the space-frequency domain, the statistical properties of a stochastic, statistically non-stationary field can be characterized by the 2×2 two-frequency, two-point CSDM, whose elements can be expressed in the form [29]

$$W_{\alpha\beta}(x_1, x_2, \omega_1, \omega_2) = \langle E_\alpha^*(x_1, \omega_1) E_\beta(x_2, \omega_2) \rangle,$$
$$(\alpha = x, y; \beta = x, y), \tag{1}$$

where E_α and E_β represent the components of the electric field along the x- and y-axes, respectively. The angular brackets denote the ensemble average. For simplicity, the analysis was limited to one spatial dimension x.

To generate a genuine beam, the CDSM must be quasi-Hermitian and exhibit non-negative definite [33]. The necessary and sufficient conditions for its elements are expressed by (2) [7], [11]:

$$W_{\alpha\beta}(x_1, x_2, \omega_1, \omega_1) = \int_{-\infty}^{\infty} \int_{-\infty}^{\infty} p_{\alpha\beta}(v_x, v_\omega)$$

$$H_\alpha^*(x_1, \omega_1; v_x, v_\omega)$$

$$\times H_\beta(x_2, \omega_2; v_x, v_\omega)\, dv_x dv_\omega, \quad (2)$$

where ω is the angular frequency, $p_{\alpha\beta}(v_x, v_\omega)$ is the elements of the 2×2 weight function matrix, and $H_\alpha(x, \omega; v_x, v_\omega)$ is an arbitrary kernel. According to [38], the following relations:

$$p_{xx}(v_x, v_\omega) \geq 0, p_{yy}(v_x, v_\omega) \geq 0,$$
$$p_{xx}(v_x, v_\omega)p_{yy}(v_x, v_\omega) - p_{xy}(v_x, v_\omega)p_{yx}(v_x, v_\omega) \geq 0, \quad (3)$$

must be obeyed for any v_x and v_ω since $p_{\alpha\beta}(v_x, v_\omega)$ is the non-negative, Fourier-transformable function. To derive the CSDM of a multi-Gaussian-correlated electromagnetic pulsed beam, the following expression was selected for $p_{\alpha\beta}(v_x, v_\omega)$ [7], [11]:

$$p_{\alpha\beta}(v_x, v_\omega) = \frac{B_{\alpha\beta}}{C_1 C_2} \sum_{n=1}^{N} \binom{N}{n} (-1)^{n-1} \sqrt{\frac{\xi_{\alpha\beta}}{\pi}} \exp\left(-\xi_{\alpha\beta} n v_x^2\right)$$

$$\times \sum_{m=1}^{M} \binom{M}{m} (-1)^{m-1} \sqrt{\frac{\eta_{\alpha\beta}}{\pi}} \exp\left(-\eta_{\alpha\beta} m v_\omega^2\right), \quad (4)$$

exhibiting the following normalization factors:

$$C_1 = \sum_{n=1}^{N} \binom{N}{n} \frac{(-1)^{n-1}}{\sqrt{n}}, \text{ and } C_2 = \sum_{m=1}^{M} \binom{M}{m} \frac{(-1)^{m-1}}{\sqrt{m}}, \quad (5)$$

where $\binom{N}{n}$ and $\binom{M}{m}$ are the binomial coefficients, N and M are the total number of terms for the muiti-Gaussian function in the spatially and temporally coherent structures, respectively. $\xi_{\alpha\beta}$ and $\eta_{\alpha\beta}$ are real constants, $B_{\alpha\beta} = |B_{\alpha\beta}|\exp(i\varphi_{\alpha\beta})$ is the correlation coefficient, and ϕ_{ij} is the phase difference. Recalling the quasi-Hermitian and non-negative definiteness, it could sufficient to hold if

$$B_{xx} = B_{yy} = 1, |B_{xy}| = |B_{yx}| \leq 1, \xi_{xy} = \xi_{yx}, \eta_{xy} = \eta_{yx}. \quad (6)$$

Substituting (4) and (6) into (3) affords the following:

$$\sqrt{\frac{\xi_{xx}}{\pi}} \sum_{n=1}^{N} \binom{N}{n} (-1)^{n-1} \exp\left(-\xi_{xx} n v_x^2\right)$$

$$\times \sqrt{\frac{\eta_{xx}}{\pi}} \sum_{m=1}^{M} \binom{M}{m} (-1)^{m-1} \exp\left(-\eta_{xx} m v_\omega^2\right)$$

$$\times \sqrt{\frac{\xi_{yy}}{\pi}} \sum_{n=1}^{N} \binom{N}{n} (-1)^{n-1} \exp\left(-\xi_{yy} n v_x^2\right)$$

$$\times \sqrt{\frac{\eta_{yy}}{\pi}} \sum_{m=1}^{M} \binom{M}{m} (-1)^{m-1} \exp\left(-\eta_{yy} m v_\omega^2\right)$$

$$\geq B_{xy}^2 \frac{\xi_{xy}}{\pi} \frac{\eta_{xy}}{\pi} \left[\sum_{n=1}^{N} \binom{N}{n} (-1)^{n-1} \exp\left(-\xi_{xy} n v_x^2\right) \times \sum_{m=1}^{M} \binom{M}{m} (-1)^{m-1} \exp\left(-\eta_{xy} m v_\omega^2\right) \right]^2, \quad (7)$$

Further, (7) can be rewritten employing the binomial theorem, as follows:

$$\sqrt{\xi_{xx}\xi_{yy}} \left\{ 1 - \left[1 - \exp\left(-\frac{\xi_{xx} v_x^2}{2}\right) \right]^N \right\}$$

$$\left\{ 1 - \left[1 - \exp\left(-\frac{\xi_{yy} v_x^2}{2}\right) \right]^N \right\}$$

$$\geq |B_{xy}| \xi_{xy} \left\{ 1 - \left[1 - \exp\left(-\frac{\xi_{xy} v_x^2}{2}\right) \right]^N \right\}^2, \quad (8.a)$$

$$\sqrt{\eta_{xx}\eta_{yy}} \left\{ 1 - \left[1 - \exp\left(-\frac{\eta_{xx} v_\omega^2}{2}\right) \right]^M \right\}$$

$$\left\{ 1 - \left[1 - \exp\left(-\frac{\eta_{yy} v_\omega^2}{2}\right) \right]^M \right\}$$

$$\geq |B_{xy}| \eta_{xy} \left\{ 1 - \left[1 - \exp\left(-\frac{\eta_{xy} v_\omega^2}{2}\right) \right]^M \right\}^2. \quad (8.b)$$

Since the weighting functions decrease monotonically, the following inequality can be easily obtained by setting $v_x = 0$ and $v_\omega = 0$:

$$\xi_{xy} \leq \frac{\sqrt{\xi_{xx}\xi_{yy}}}{|B_{xy}|}, and\, \mu_{xy} \leq \frac{\sqrt{\eta_{xx}\eta_{yy}}}{|B_{xy}|}, \quad (9)$$

after which (8) can be simplified, as follows:

$$\min \left\{ 1 - \left[1 - \exp\left(-\frac{\xi_{xx} v_x^2}{2}\right) \right]^N, \right.$$

$$\left. 1 - \left[1 - \exp\left(-\frac{\xi_{yy} v_x^2}{2}\right) \right]^N \right\}$$

$$\geq 1 - \left[1 - \exp\left(-\frac{\xi_{xy} v_x^2}{2}\right) \right]^N, \quad (10.a)$$

$$\min \left\{ 1 - \left[1 - \exp\left(-\frac{\eta_{xx} v_\omega^2}{2}\right) \right]^M, \right.$$

$$\left. 1 - \left[1 - \exp\left(-\frac{\eta_{yy} v_\omega^2}{2}\right) \right]^M \right\}$$

$$\geq 1 - \left[1 - \exp\left(-\frac{\eta_{xy}v_\omega^2}{2}\right)\right]^M, \quad (10.b)$$

indicating that

$$\xi_{xy} \geq \max\left(\xi_{xx}, \xi_{yy}\right), and\, \eta_{xy} \geq \max\left(\eta_{xx}, \eta_{yy}\right). \quad (11)$$

Combining inequalities (9) and (11), can obtain the following double inequality without the loss of generality:

$$\max\left(\xi_{xx}, \xi_{yy}\right) \leq \xi_{xy} \leq \frac{\sqrt{\xi_{xx}\xi_{yy}}}{|B_{xy}|},$$

$$and \max\left(\eta_{xx}, \eta_{yy}\right) \leq \eta_{xy} \leq \frac{\sqrt{\eta_{xx}\eta_{yy}}}{|B_{xy}|}. \quad (12)$$

Notably, (12) is independent regarding the parameter, N or M, as expected in [22], [23], which tighter than that of the classical EGSM source in [39] for N (or M) = 1.

Regarding the Schell-model sources, the kernel $H_\alpha\, (x, \omega; v_x, v_\omega)$ must exhibit a Fourier-like structure [22], i.e.,

$$H_\alpha\left(x_1, \omega_1; v_x, v_\omega\right) = A_\alpha K\left(x_1, \omega_1\right)\exp\left(-iv_x \cdot x_1\right)$$
$$\times \exp\left(-iv_\omega \cdot \omega_1\right), \quad (13.a)$$

$$H_\beta\left(x_2, \omega_2; v_x, v_\omega\right) = A_\beta K\left(x_2, \omega_2\right)\exp\left(-iv_x \cdot x_2\right)$$
$$\times \exp\left(-iv_\omega \cdot \omega_2\right), \quad (13.b)$$

where $K(x, \omega)$ denotes the spectral-density distribution of the source. Thereafter, (2) indicates that the CSDM assumes the following form:

$$W_{\alpha\beta}\left(x_1, x_2, \omega_1, \omega_2\right) = A_\alpha A_\beta K^*\left(x_1, \omega_1\right)K\left(x_2, \omega_2\right)$$
$$\times g_{\alpha\beta}\left(x_1 - x_2, \omega_1 - \omega_2\right), \quad (14)$$

where $g_{\alpha\beta}$ is the degree of coherence (DOC) of the source. Further, CSDM represents an EGSMP source if $K(x, \omega)$ and $p_{\alpha\beta}$ (v_x, v_ω) are Gaussian functions.

To generate twisted EMGSMP beams, we assumed that the kernel is in the following form [7], [9], [11]:

$$H_\alpha\left(x, \omega; v_x, v_\omega\right) = A_\alpha \exp\left(-\frac{x^2}{\sigma_x^2}\right)\exp\left(-\frac{\bar{\omega}^2}{\sigma_\omega^2}\right)$$
$$\times \exp\left\{-\left[(a\bar{\omega} + ix)v_x - (bx - i\bar{\omega})v_\omega\right]\right\}, \quad (15)$$

where A_α is the amplitude of the field component, $\bar{\omega} = \omega - \omega_0$ and ω_0 is the central angular frequency of the carrier wave. σ_x and σ_ω are the rms beam and pulse spectral widths along the x- and ω-direction, respectively. a and b are the positive real constants.

The CSDM can be expressed by substituting (4) and (15) into (1):

$$W_{\alpha\beta}\left(x_1, x_2, \omega_1, \omega_2\right) = \frac{A_\alpha A_\beta B_{\alpha\beta}}{C_1 C_2}\sum_{n=1}^{N}\binom{N}{n}\frac{(-1)^{n-1}}{\sqrt{n}}$$

$$\times \exp\left[-\left(\frac{1}{\sigma_\omega^2} - \frac{\xi_{\alpha\beta}\mu_{\alpha\beta}^2}{2n}\right)\left(\bar{\omega}_1^2 + \bar{\omega}_2^2\right) - \frac{(x_1 - x_2)^2}{4n\xi_{\alpha\beta}}\right.$$

$$\left.- \frac{\xi_{\alpha\beta}\mu_{\alpha\beta}^2(\bar{\omega}_1 - \bar{\omega}_2)^2}{4n}\right]\times \exp\left[-i\mu_{\alpha\beta}\frac{(x_1 - x_2)(\bar{\omega}_1 + \bar{\omega}_2)}{2n}\right]$$

$$\times \sum_{m=1}^{M}\binom{M}{m}\frac{(-1)^{m-1}}{\sqrt{m}} \times \exp\left[-\left(\frac{1}{\sigma_x^2} - \frac{\eta_{\alpha\beta}\mu_{\alpha\beta}^2}{2m}\right)\left(x_1^2 + x_2^2\right)\right.$$

$$\left.- \frac{(\bar{\omega}_1 - \bar{\omega}_2)^2}{4m\eta_{\alpha\beta}} - \frac{\eta_{\alpha\beta}\mu_{\alpha\beta}^2(x_1 - x_2)^2}{4m}\right]$$

$$\times \exp\left[-i\mu_{\alpha\beta}\frac{(x_1 + x_2)(\bar{\omega}_1 - \bar{\omega}_2)}{2m}\right], \quad (16)$$

with the following twisted factor:

$$\mu_{\alpha\beta} = \frac{a}{\xi_{\alpha\beta}} = \frac{b}{\eta_{\alpha\beta}}. \quad (17)$$

Notably, σ_x and σ_ω did not represent the beam size and spectral width, which were also affected by the twisted factor, $\mu_{\alpha\beta}$, respectively. At N and $M = 1$, we observed the following:

$$W_{\alpha\beta}\left(x_1, x_2, \omega_1, \omega_1\right) = A_\alpha A_\beta B_{\alpha\beta}\exp\left(-\frac{x_1^2 + x_2^2}{4w_{x\_\alpha\beta}^2}\right)$$

$$\times \exp\left[-\frac{(x_1 - x_2)^2}{2\delta_{\alpha\beta}^2}\right]\exp\left(-\frac{\bar{\omega}_1^2 + \bar{\omega}_2^2}{4w_{\omega\_\alpha\beta}^2}\right)$$

$$\times \exp\left[-\frac{(\bar{\omega}_1 - \bar{\omega}_2)^2}{2\Omega_{\alpha\beta}^2}\right]\times \exp\left[i\mu_{\alpha\beta}\left(x_2\bar{\omega}_1 - x_1\bar{\omega}_2\right)\right], \quad (18)$$

with

$$\frac{1}{4w_{x\_\alpha\beta}^2} = \frac{1}{\sigma_x^2} - \frac{\eta_{\alpha\beta}\mu_{\alpha\beta}^2}{2}, \frac{1}{4w_{\omega\_\alpha\beta}^2} = \frac{1}{\sigma_\omega^2} - \frac{\xi_{\alpha\beta}\mu_{\alpha\beta}^2}{2},$$

$$\frac{1}{2\delta_{\alpha\beta}^2} = \frac{\eta_{\alpha\beta}\mu_{\alpha\beta}^2}{4} + \frac{1}{4\xi_{\alpha\beta}}, \frac{1}{2\Omega_{\alpha\beta}^2} = \frac{\xi_{\alpha\beta}\mu_{\alpha\beta}^2 a^2}{4} + \frac{1}{4\eta_{\alpha\beta}}. \quad (19)$$

$w_{x\_\alpha\beta}$ and $w_{\omega\_\alpha\beta}$ are the beam and spectral widths of the pulsed source, respectively, and $\delta_{\alpha\beta}$ and $\Omega_{\alpha\beta}$ are the spatial and spectral-coherence widths, respectively. According to [7], $\mu_{\alpha\beta}$ which must satisfy the inequality, is given, as follows:

$$|\mu_{\alpha\beta}| \leq \frac{1}{\delta_{\alpha\beta}\Omega_{\alpha\beta}}. \quad (20)$$

Equation (16) denotes a new family of sources exhibiting a multi-Gaussian correlation function; they may be named the twisted EMGSMP sources. Equation (18) corresponds to the twisted EGSMP sources; their rotations are along the x–ω plane. Compared with the CSD function of the scalar twisted space-frequency GSM sources, which were introduced in [7], (16) can be considered as the electromagnetic counterpart. Additionally, if $\mu_{\alpha\beta}$ is set to be zero, it would become an EMGSMP beam.

II. FORMULAS FOR THE PROFAGATION OF THE TWISTED EMGSMP SOURCES

Assuming that the source in (16) propagates through an ABCD optical system based on the extended Collins formula, the elements of CSDM can be expressed, as reported in [40]:

$$W_{\alpha\beta}(x_1, x_2, z, \omega_1, \omega_2) = \frac{\sqrt{\omega_1\omega_2}}{2\pi cB}\exp\left[\frac{i(\omega_1 - \omega_2)z}{c}\right]$$
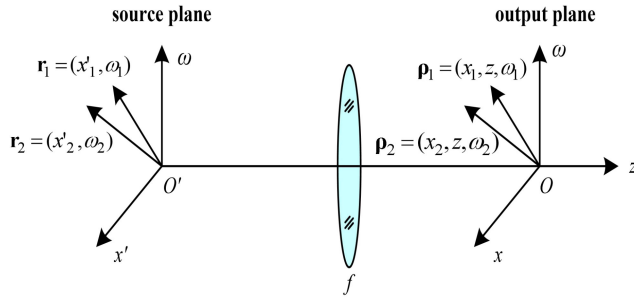
Fig. 1. Geometry and notation relating to the propagation of the twisted electromagnetic pulsed source through the ABCD optical system.

$$\times \int\int_{-\infty}^{\infty} dx'_1 dx'_2 W_{\alpha\beta}(x'_1, x'_2, \omega_1, \omega_2)$$

$$\times \exp\left[\frac{i\omega_1}{2cB}\left(Ax'^2_1 - 2x'_1 \cdot x_1 + Dx_1^2\right) - \frac{i\omega_2}{2cB}\right.$$

$$\left.\left(Ax'^2_2 - 2x'_2 \cdot x_2 + Dx_2^2\right)\right], \tag{21}$$

where x_1 and x_2 are the transverse position coordinates of the two arbitrary points along the output plane, z. A, B, C, and D are the matrix elements of the optical system between the source and output planes. Fig. 1 shows the geometry and notation relating to the propagation of the twisted electromagnetic pulsed source through the ABCD optical system.

The elements of the CSDM along the output plane can be expressed by (22) by substituting (16) into (21) and calculating the integral:

$$W_{\alpha\beta}(x_1, x_2, z, \omega_1, \omega_2) = \frac{A_\alpha A_\beta B_{\alpha\beta}\sqrt{\omega_1\omega_2}}{2\pi cBC_1 C_2} \exp\left[\frac{i(\omega_1 - \omega_2)z}{c}\right]$$

$$\times \exp\left[\frac{iD}{2cB}\left(\omega_1 x_1^2 - \omega_2 x_2^2\right)\right] \times \sum_{n=1}^{N}\binom{N}{n}\frac{(-1)^{n-1}}{\sqrt{n}}\sum_{m=1}^{M}\binom{M}{m}$$

$$\frac{(-1)^{m-1}}{\sqrt{m}}$$

$$\times \sqrt{\frac{4\pi^2}{4Q_{1\alpha\beta}Q_{2\alpha\beta} - R_{\alpha\beta}^2}} \exp\left[-\frac{g_{\alpha\beta}^2 Q_{2\alpha\beta} + h_{\alpha\beta}^2 Q_{1\alpha\beta} - g_{\alpha\beta}h_{\alpha\beta}R_{\alpha\beta}}{4Q_{1\alpha\beta}Q_{2\alpha\beta} - R_{\alpha\beta}^2}\right]$$

$$\times \exp\left[-\left(\frac{1}{\sigma_\omega^2} - \frac{\xi_{\alpha\beta}\mu_{\alpha\beta}^2}{2n}\right)(\bar{\omega}_1^2 + \bar{\omega}_2^2)\right.$$

$$\left.-\left(\frac{1}{4m\eta_{\alpha\beta}} + \frac{\xi_{\alpha\beta}\mu_{\alpha\beta}^2}{4n}\right)(\bar{\omega}_1 - \bar{\omega}_2)^2\right], \tag{22}$$

where

$$\begin{cases} Q_{1\alpha\beta} = \frac{1}{\sigma_x^2} - \frac{\eta_{\alpha\beta}\mu_{\alpha\beta}^2}{2m} + \frac{1}{4n\xi_{\alpha\beta}} + \frac{\eta_{\alpha\beta}\mu_{\alpha\beta}^2}{4m} - \frac{i\omega_1}{2cB}A, \\ Q_{2\alpha\beta} = \frac{1}{\sigma_x^2} - \frac{\eta_{\alpha\beta}\mu_{\alpha\beta}^2}{2m} + \frac{1}{4n\xi_{\alpha\beta}} + \frac{\eta_{\alpha\beta}\mu_{\alpha\beta}^2}{4m} + \frac{i\omega_2}{2cB}A, \\ R_{\alpha\beta} = \frac{1}{2n\xi_{\alpha\beta}} + \frac{\eta_{\alpha\beta}\mu_{\alpha\beta}^2}{2m}, \\ g_{\alpha\beta} = \frac{\omega_1}{cB}x_1 + \mu_{\alpha\beta}\left(\frac{1}{2n} - \frac{1}{2m}\right)\bar{\omega}_1 + \mu_{\alpha\beta}\left(\frac{1}{2n} + \frac{1}{2m}\right)\bar{\omega}_2, \\ h_{\alpha\beta} = \frac{\omega_2}{cB}x_2 + \mu_{\alpha\beta}\left(\frac{1}{2n} + \frac{1}{2m}\right)\bar{\omega}_1 + \mu_{\alpha\beta}\left(\frac{1}{2n} - \frac{1}{2m}\right)\bar{\omega}_2. \end{cases} \tag{23}$$

The spectral density along the output plane can be obtained by evaluating (22) at the same space and frequency points, i.e.,

$$S(x, z, \omega)$$

$$= \frac{\omega}{cBC_1 C_2}\sum_{n=1}^{N}\binom{N}{n}\frac{(-1)^{n-1}}{\sqrt{n}}\sum_{m=1}^{M}\binom{M}{m}\frac{(-1)^{m-1}}{\sqrt{m}}$$

$$\times \left\{\frac{A_x^2}{\sqrt{4Q_{1xx}Q_{2xx} - R_{xx}^2}} \exp\left[-\left(\frac{1}{\sigma_\omega^2} - \frac{\xi_{xx}\mu_{xx}^2}{2n}\right)\bar{\omega}^2\right]\right.$$

$$\times \exp\left[-\frac{g_{xx}^2 Q_{2xx} + h_{xx}^2 Q_{1xx} - g_{xx}h_{xx}R_{xx}}{4Q_{1xx}Q_{2xx} - R_{xx}^2}\right]$$

$$+ \frac{A_y^2}{\sqrt{4Q_{1yy}Q_{2yy} - R_{yy}^2}} \exp\left[-\left(\frac{1}{\sigma_\omega^2} - \frac{\xi_{yy}\mu_{yy}^2}{2n}\right)\bar{\omega}^2\right]$$

$$\left.\times \exp\left[-\frac{g_{yy}^2 Q_{2yy} + h_{yy}^2 Q_{1yy} - g_{yy}h_{yy}R_{yy}}{4Q_{1yy}Q_{2yy} - R_{yy}^2}\right]\right\}, \tag{24}$$

where

$$\begin{cases} Q_{1\alpha\beta} = \frac{1}{\sigma_x^2} - \frac{\eta_{\alpha\beta}\mu_{\alpha\beta}^2}{2m} + \frac{1}{4n\xi_{\alpha\beta}} + \frac{\eta_{\alpha\beta}\mu_{\alpha\beta}^2}{4m} - \frac{i\omega}{2cB}A, \\ Q_{2\alpha\beta} = \frac{1}{\sigma_x^2} - \frac{\eta_{\alpha\beta}\mu_{\alpha\beta}^2}{2m} + \frac{1}{4n\xi_{\alpha\beta}} + \frac{\eta_{\alpha\beta}\mu_{\alpha\beta}^2}{4m} + \frac{i\omega}{2cB}A, \\ R_{\alpha\beta} = \frac{1}{2n\xi_{\alpha\beta}} + \frac{\eta_{\alpha\beta}\mu_{\alpha\beta}^2}{2m}, g_{\alpha\beta} = \frac{\omega}{cB}x + \frac{\mu_{\alpha\beta}}{n}\bar{\omega}, \\ h_{\alpha\beta} = \frac{\omega}{cB}x + \frac{\mu_{\alpha\beta}}{m}\bar{\omega}. \end{cases} \tag{25}$$

The spectral intensity of the twisted EMGSMP beam is determined by (24), and the spectral property during propagation was studied by selecting the parameters of the source.

The correlations between the different electric-field frequency components are characterized by the spectral DOC $\mu_{EM}(x_1, x_2, z, \omega_1, \omega_2)$, which takes the following form [41]:

$$\mu_{EM}(x_1, x_2, z, \omega_1, \omega_2) = \frac{\|W_{\alpha\beta}(x_1, x_2, z, \omega_1, \omega_2)\|_F}{\sqrt{S(x_1, z, \omega_1)}\sqrt{S(x_2, z, \omega_2)}}, \tag{26}$$

where $\|\cdot\|_F$ is the Frobenius norm.

IV. EVOLUTION OF THE SPECTRAL AND COHERENCE PROPERTIES OF THE TWISTED EMGSMP SOURCES DURING PROPAGATION

In this section, we numerically calculated the spectral intensity and coherence of the twisted EMGSMP source employing the preceding analyses. Thus, we assumed that the source beam passes through a thin lens with focal length, f, and arrives at the output plane. The ray matrix of such an optical system can be expressed, as follows, according to [42]:

$$\begin{bmatrix} A & B \\ C & D \end{bmatrix} = \begin{bmatrix} 1 & z \\ 0 & 1 \end{bmatrix}\begin{bmatrix} 1 & 0 \\ -\frac{1}{f} & 1 \end{bmatrix}$$

$$\begin{bmatrix} 1 & f \\ 0 & 1 \end{bmatrix} = \begin{bmatrix} 1 - \frac{z}{f} & f \\ -\frac{1}{f} & 0 \end{bmatrix}, \tag{27}$$

The parameters in the following calculations were set as $\lambda_0 = 632.8$ nm, $A_x = 1$, $A_y = 1.5$, $B_{xy} = 0$, $\sigma_x = 0.3$ mm, $\sigma_\omega = 37.8$ GHz, and f = 150 mm; the other parameters were specified in the figure captions.

A. Spectral Intensity

First, we focused on the evolution of the spectral properties during propagation. For $\mu_{xx} = \mu_{yy} = \mu$, Fig. 2 shows the contour of the normalized spectral density of the twisted EMGSMP
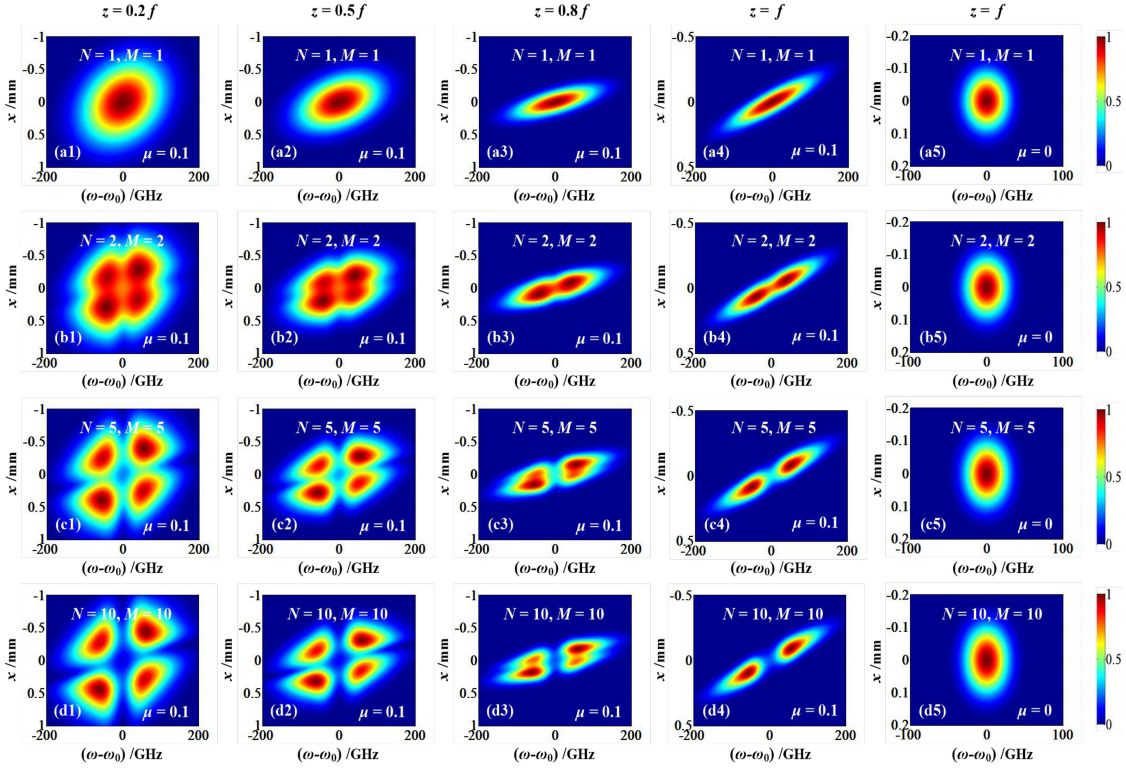
Fig. 2. Normalized spectral density distribution of a focused twisted EMGSMP source at different propagating distances for different values of N and M. For (a1-a4), (b1-b4), (c1-c4), (d1-d4) $\mu_{xx} = \mu_{yy} = \mu = 0.1$ (mm.GHz)$^{-1}$, $\xi_{xx} = \xi_{yy} = \xi = 0.13$ mm^2 and $\eta_{xx} = \eta_{yy} = \eta = 0.002$ THz^2 ; and (a5, b5, c5, d5) $\mu = 0$ (mm.GHz)$^{-1}$.

TABLE I
SIMULATED PARAMETERS IN FIG. 2

Parameter	Value	Unit
$\mu_{xx} = \mu_{yy} = \mu$	0.1	(mm·GHz)$^{-1}$
$\xi_{xx} = \xi_{yy} = \xi$	0.13	mm^2
$\eta_{xx} = \eta_{yy} = \eta$	0.002	THz^2
$w_{x\_xx} = w_{x\_yy} = w_x$	0.5	mm
$w_{\omega\_xx} = w_{\omega\_yy} = w_\omega$	70.7	GHz
$\delta_{xx} = \delta_{yy} = \delta$	0.269	mm
$\Omega_{xx} = \Omega_{yy} = \Omega$	33.3	GHz

beam which was focused by a thin lens at several propagation distances for different values of total numbers of terms (N and M). For comparison, the twist factors in Fig. 2 were set as 0.1 (mm.GHz)$^{-1}$ from the first to the fourth columns and 0 (mm.GHz)$^{-1}$ in the fifth column, respectively. Other simulated parameters are shown in Table I. As expected, the $\mu_{\alpha\beta}$ has a remarkable effect on the spectral density distribution. One can find that for the MGSMP beam without twist factor [Figs. 2(a5), (b5), (c5), and (d5)], the normalized spectral distribution possesses a Gaussian-like profile in the focal plane. However, the twisted EMGSMP beam, for which $\mu \neq 0$, shows a different picture [Figs. 2(a1–a4), (b1–b4), (c1–c4), and (d1–d4)]. For the case of $N = 1$ and $M = 1$, the normalized spectral density distribution of the conventional GSMP beam with a $\mu_{\alpha\beta}$ rotates and the beam size gradually decreases in the longitude direction during transmission. The result is in line with the results of the previous investigation [7]. For the case of $N > 1$ and M

> 1, it is shown that the initial Gaussian spectral density splits into a rotating four-lobe array profile, and the distance between each lobe grows as total numbers of terms increase. However, with the increase of the propagation distance, the beam spot in the transverse direction gradually disappears, and eventually it exhibits a rotating two-lobe shaped in the focal plane.

The physical interpretation is thus: for an EMGSMP beam without the twist factor, a Fourier-like relation existed between the spectral density in the focal plane and the initial distribution [29]. However, regarding the twisted EMGSMP beam, this reciprocal relationship disappeared owing to the presence of the twist factor [29], [42]. This is because the twist factor causes a focal shift, which results in beam rotation and destroys the spatial and spectral coherences of the beam, thereby affecting the beam characteristics during transmission. The EMGSMP beam, with no spatiotemporal coupling, is unchanged and diffracts in the x- and ω-dimension, respectively. As a result, the orientations of the beam profiles do not change. Conversely, for the twisted EMGSMP beam, spatiotemporal coupling causes diffraction to affect both the spatial and pulse widths of the beam. The relationship between these widths and the subsequent redistribution of intensity manifests as beam rotation and split during transmission.

For the case involving $\mu_{xx} \neq \mu_{yy}$, Fig. 3 shows the contour of the normalized spectral density distribution of the twisted EMGSMP beam which was focused by a thin lens at several propagation distances for different values of the total numbers of terms N and M. The simulated parameters are listed in Table II. Similarly, regarding the twisted EMGSMP source, Fig. 3 indicates that a rotating two-lobe-shaped beam was available along the focal plane, and this is a significant feature that
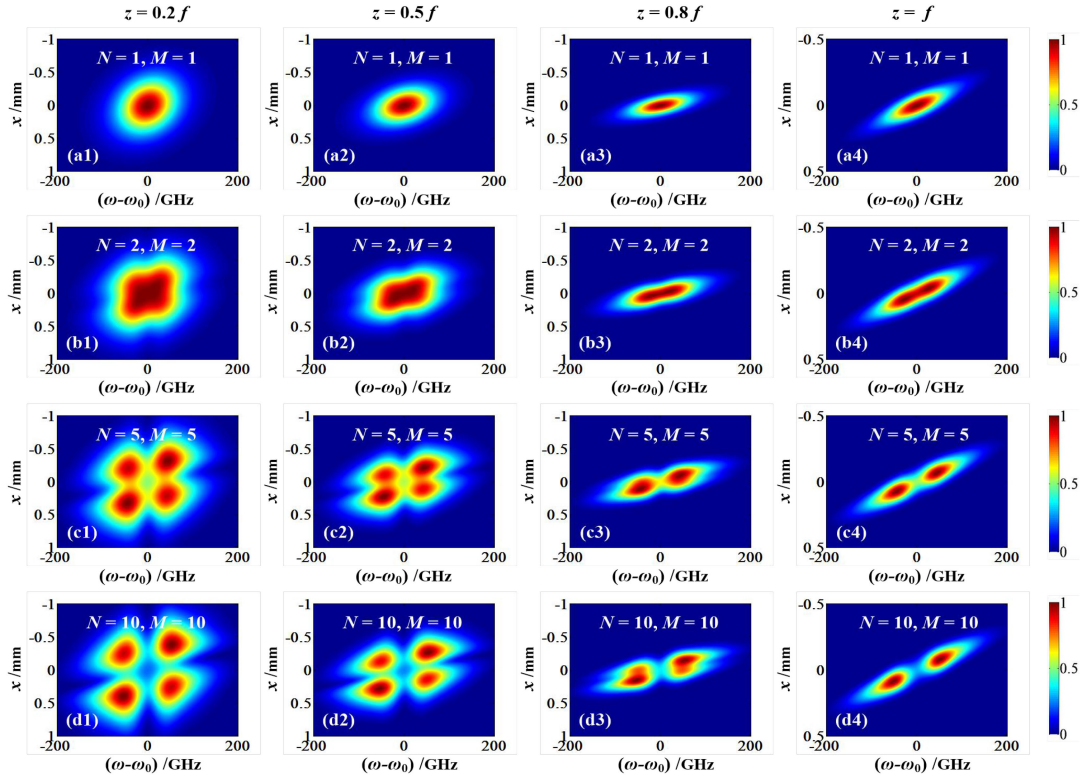
Fig. 3. Normalized spectral density distribution of a focused twisted EMGSMP source at different propagating distances for different values of N and M. For μ_{xx} = 0.1 (mm.GHz)$^{-1}$, and μ_{yy} = 0.08 (mm.GHz)$^{-1}$.

TABLE II
SIMULATED PARAMETERS IN FIG. 3

Parameter	Value	Unit
μ_{xx}	0.1	(mm·GHz)$^{-1}$
μ_{yy}	0.08	(mm·GHz)$^{-1}$
ξ_{xx}	0.13	mm^2
ξ_{yy}	0.1625	mm^2
η_{xx}	0.002	THz^2
η_{yy}	0.0025	THz^2
w_{x_xx}	0.5	mm
w_{x_yy}	0.5	mm
w_{ω_xx}	70.7	GHz
w_{ω_yy}	37.3	GHz
δ_{xx}	0.269	mm
δ_{yy}	0.3	mm
Ω_{xx}	33.3	GHz
Ω_{yy}	31.4	GHz

differentiates the twisted EMGSMP beam source from the non-twisted one. Compared with the case of $\mu_{xx} = \mu_{yy}$, this beam evolves more slowly during transmission.

Fig. 4 shows the plots of the normalized spectral density of the twisted EMGSMP source at several radial coordinates (x) along the focal plane for different values of the total numbers of terms N and M. The on-axis normalized spectral density distribution of the twisted EMGSMP source is consistent with

the initial spectrum distribution, which gradually split into a bimodal structure as the total numbers of terms N and M increase; the width of the beam is smaller than the initial beam size. Compared with the on-axis spectrum, the off-axis one shifts toward the direction of the smaller frequency, i.e., a red shift. Moreover, the spectral switch interestingly occurred during transmission and was closely related to the total numbers of terms N and M.

B. Spectral DOC

Next, we examined the evolution of the modulus of the two-frequency, two-point spectral DOC, $|\mu_{EM}(x, 0, z, \omega_1 - \omega_2)|$, of the focused twisted EMGSMP source during transmission, and employed (22) and (26) to compute $|\mu_{EM}(x, 0, z, \omega_1 - \omega_2)|$; the results are plotted in Figs. 5 and 6. Fig. 5 shows the evolution of $|\mu_{EM}(x, 0, z, \omega_1 - \omega_2)|$ of the focused EGSMP source ($N = M = 1$) with a $\mu_{\alpha\beta}$ or a non-$\mu_{\alpha\beta}$ at different propagation distances. Similar to the spectral density, the spectral DOC rotated during transmission, and the rotation angle depended on the value of $\mu_{\alpha\beta}$. Fig. 6 shows the evolution of $|\mu_{EM}(x, 0, z, \omega_1 - \omega_2)|$ of the focused EMGSMP source ($N = M = 10$) with a $\mu_{\alpha\beta}$ or a non-$\mu_{\alpha\beta}$, it could be observed that the spectral DOC structure depended on the twist factor, as well as the total numbers of terms N and M. Moreover, the existence of the $\mu_{\alpha\beta}$ rotated the spectral coherence structure, and distorted its shaped. It was observed that the spectral DOC structure of a focused twisted EMGSMP source does not exhibit a symmetry profile at that point; it exhibited a counterclockwise rotation with the increasing propagation distance. Thus, the spectral DOC of the
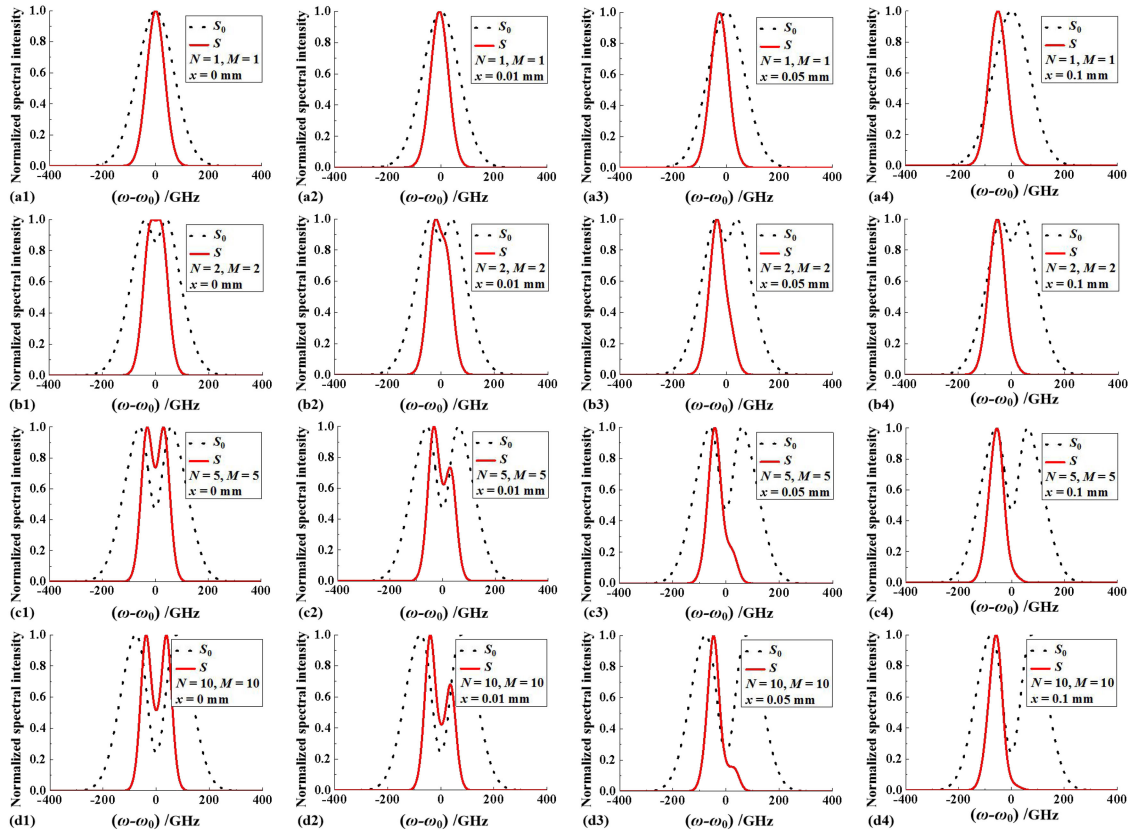
Fig. 4. Evolution of the normalized spectral density distribution of a twisted EMGSMP source as a function of $(\omega-\omega_0)$ in the focal plane. The black dot curves denote the original normalized spectrum S_0. The simulated parameters were assumed to be the same as in Fig. 2.
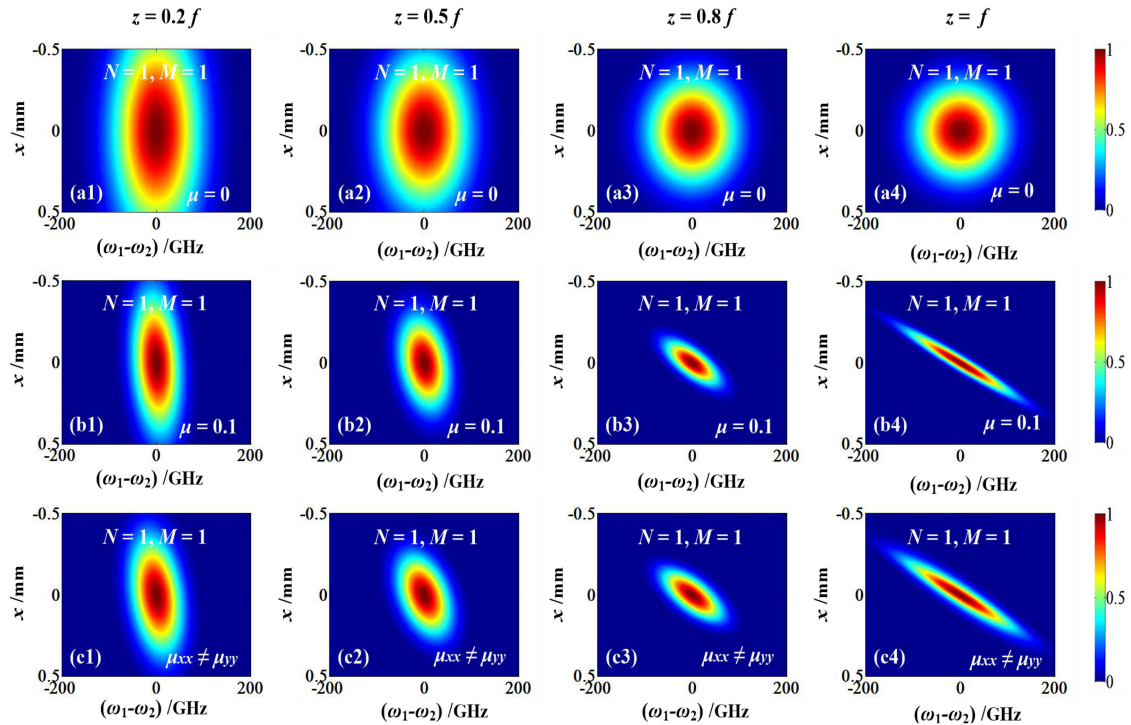

Fig. 5. Evolution of the modulus of the spectral degree of coherence (DOC) of a focused twisted EGSMP source as several propagation distances for different values of twisted factor. The simulated parameters were assumed to be the same as in Figs. 2 and 3.
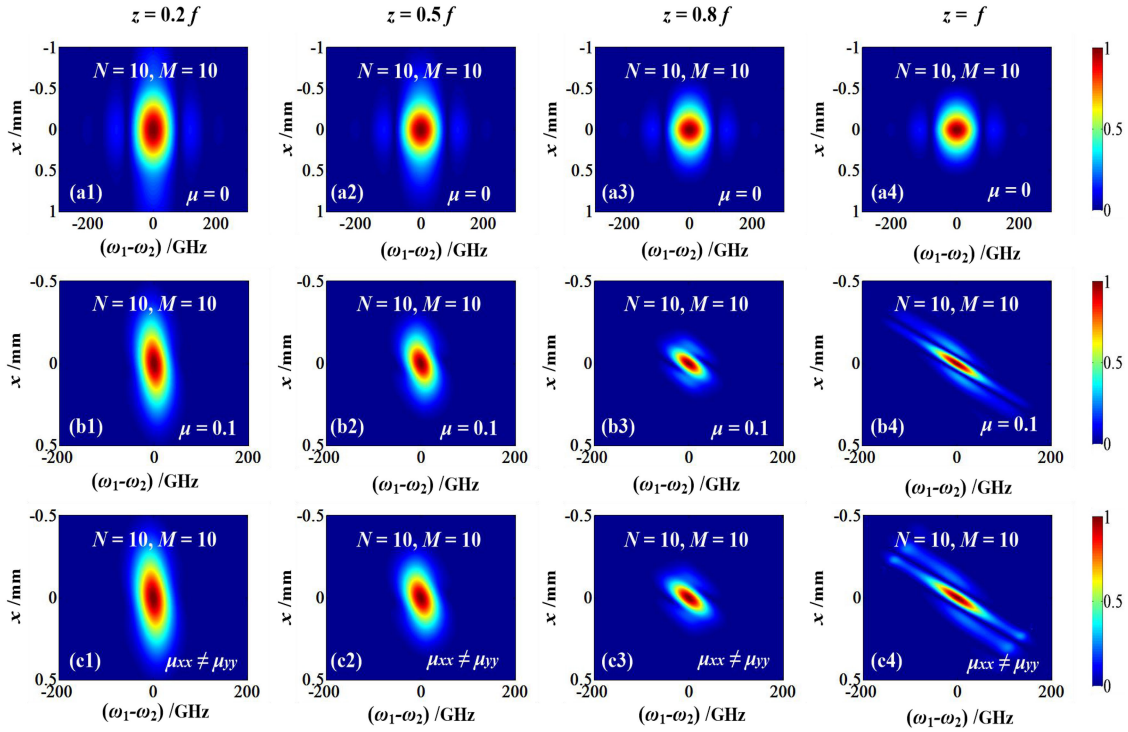
Fig. 6. Evolution of the modulus of the spectral DOC of a focused twisted EMGSMP source at several different propagation distances for the different values of $\mu_{\alpha\beta}$. The simulated parameters were assumed to be the same as in Figs. 2 and 3.
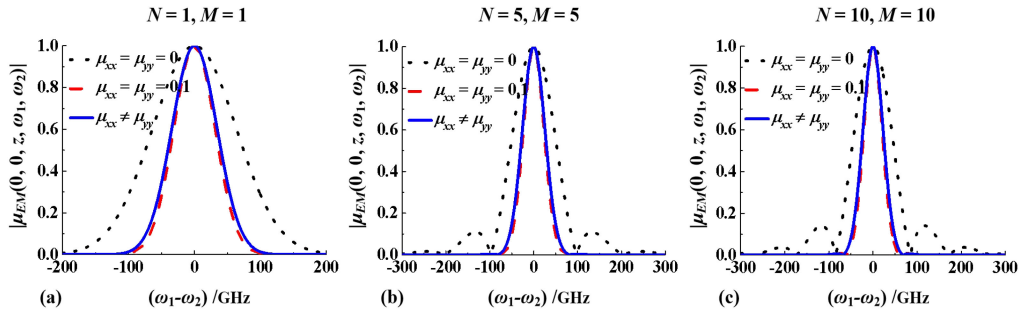

Fig. 7. Evolution of the modulus of the on-axis two-frequency, single-point DOC of the twisted EMGSMP source along the focal plane for different values of $\mu_{\alpha\beta}$. The simulated parameters were assumed to be the same as in Figs. 2 and 3.

twisted EMGSMP beam was notably different from that without $\mu_{\alpha\beta}$ during transmission.

Finally, to elucidate the spectral coherence property, Fig. 7 shows the plots of the modulus of the on-axis two-frequency, single-point spectral DOC ($|\mu_{EM}(0, 0, z = f, \omega_1 - \omega_2)|$) distribution of the EMGSMP source with and without $\mu_{\alpha\beta}$ along the focal plane. As observed, $\mu_{\alpha\beta}$ was key to the width of the spectral coherence. Additionally, since the two-frequency, single-point cross-spectral density function and the two-time, single-point mutual coherence function are Fourier-transform pairs, we inferred that the temporal coherence of the focused twisted EMGSMP source is also closely related to $\mu_{\alpha\beta}$.

V. CONCLUSION

We introduced a novel family of twisted EMGSMP sources exhibiting transverse OAM. The spatial- and spectral-coherence

distributions of the sources could be described by a multi-Gaussian function. Further, the realizability conditions for such sources were determined. Additionally, the analytical formulas of the CSDM of such beams propagating through a thin lens were derived; they were employed to discuss the spectral and coherence properties of the twisted EMGSMP sources during transmission. The behaviors of the twisted and non-twisted EMGSMP beams were notably different. For example, their spectral densities split into a rotating four-lobe array profile near the source plane, and eventually exhibited a rotating two-lobe shaped along the focal plane, and the distance between each lobe increased as the total numbers of terms N and M increased. Their spectral DOC structures no longer exhibited a symmetry profile, and they displayed a counterclockwise rotation as the propagation distance increased. Compared with the on-axis spectrum, the off-axis one shifted toward the smaller frequency, i.e., a red shift. Moreover, the spectral switch interestingly occurred during transmission and was closely related to the total numbers

of terms of the multi-Gaussian correlated source, N and M. It can be concluded that it is feasible to generate such beams by modulating both the spatial and temporal coherence functions, as well as $\mu_{\alpha\beta}$. This availed a method for synthesizing fields exhibiting transverse OAM with peculiar spectral and coherence structures. Since the twisted EMGSMP beam exhibited a higher degree of freedom than the conventional GSMP beam, it might exhibit different potential applications in many fields.

REFERENCES

[1] A. M. Yao and M. J. Padgett, "Orbital angular momentum: Origins, behavior and applications," *Adv. Opt. Photon.*, vol. 3, no. 2, pp. 161–204, Jun. 2011, doi: 10.1364/AOP.3.000161.

[2] Y. J. Shen *et al.*, "Optical vortices 30 years on: OAM manipulation from topological charge to multiple singularities," *Light Sci. Appl.*, vol. 8, no. 1, pp. 90, Oct. 2019, doi: 10.1038/s41377-019-0194-2.

[3] R. Chen *et al.*, "Orbital angular momentum waves: Generation, detection and emerging applications," *IEEE Commun. Surv. Tut.*, vol. 22, no. 2, pp. 840–868, Nov. 2020, doi: 10.1109/COMST.2019.2952453.

[4] A. E. Willner *et al.*, "Recent advances in high-capacity free-space optical and radio-frequency communications using orbital angular momentum multiplexing," *Phil. Trans. R. Soc. A*, vol. 375, no. 2087, Feb. 2017, Art. no. 20150439, doi: 10.1098/rsta.2015.0439.

[5] M. Padgett and R. Bowman, "Tweezers with a twist," *Nat. Photon.*, vol. 5, no. 6, pp. 343–348, May 2011, doi: 10.1038/nphoton.2011.81.

[6] R. Simon and N. Mukunda, "Twisted Gaussian Schell-model beams," *J. Opt. Soc. Amer. A*, vol. 10, no. 1, pp. 95–109, Jan. 1993, doi: 10.1364/JOSAA.10.000095.

[7] M. W. Hyde, "Twisted space-frequency and spacetime partially coherent beams," *Sci. Rep.*, vol. 10, no. 1, Jul. 2020, Art. no. 12443, doi: 10.1038/s41598-020-68705-9.

[8] R. Borghi, F. Gori, G. Guattar, and M. Santarsiero, "Twisted Schell-model beams with axial symmetry," *Opt. Lett.*, vol. 40, no. 19, pp. 4504–4507, Oct. 2015, doi: 10.1364/OL.40.004504.

[9] Z. Mei and O. Korotkova, "Random sources for rotating spectral densities," *Opt. Lett.*, vol. 42, no. 2, pp. 255–258, Jan. 2017, doi: 10.1364/OL.42.000255.

[10] F. Gori and M. Santarsiero, "Devising genuine twisted cross-spectral densities," *Opt. Lett.*, vol. 43, no. 3, pp. 595–598, Feb. 2018, doi: 10.1364/OL.43.000595.

[11] Z. Mei and O. Korotkova, "Twisted EM beams with structured correlations," *Opt. Lett.*, vol. 43, no. 16, pp. 3905–3908, Aug. 2018, doi: 10.1364/OL.43.003905.

[12] X. F. Peng *et al.*, "Twisted Laguerre-Gaussian Schell-model beam and its orbital angular moment," *Opt. Exp.*, vol. 26, no. 26, pp. 33956–33969, Dec. 2018, doi: 10.1364/OE.26.033956.

[13] L. P. Wan and D. M. Zhao, "Twisted Gaussian Schell-model array beams," *Opt. Lett.*, vol. 43, no. 15, pp. 3554–3557, Aug. 2018, doi: 10.1364/OL.43.003554.

[14] M. M. Tang, H. H. Li, and X. Z. Li, "Propagation of twisted EM Gaussian Schell-model array beams in anisotropic turbulence," *Appl. Opt.*, vol. 59, no. 11, pp. 3432–3439, Apr. 2020, doi: 10.1364/AO.389577.

[15] Y. Wang *et al.*, "Twisted elliptical multi-Gaussian Schell-model beams and their propagation properties," *J. Opt. Soc. Amer. A*, vol. 37, no. 1, pp. 89–97, Jan. 2020, doi: 10.1364/JOSAA.37.000089.

[16] M. W. Hyde, "Twisted spatiotemporal optical vortex random fields," *IEEE Photon. J.*, vol. 13, no. 2, Apr. 2021, Art. no. 6500116, doi: 10.1109/JPHOT.2021.3066898.

[17] A. P. Sukhorukov and V. V. Yangirova, "Spatio-temporal vortices: Properties, generation and recording," in *Proc. Congr. Opt. Optoelectron.*, Warsaw, Poland, 2005, vol. 5949, pp. 35–43, doi: 10.1117/12.623906.

[18] K. Y. Bliokh and F. Nori, "Spatiotemporal vortex beams and angular momentum," *Phys. Rev. A*, vol. 86, no. 3, Sep. 2012, Art. no. 033824, doi: 10.1103/PhysRevA.86.033824.

[19] N. Jhajj *et al.*, "Spatiotemporal optical vortices," *Phys. Rev. X*, vol. 6, no. 3, 2016, Art. no. 031037, doi: 10.1103/PhysRevX.6.031037.

[20] S. W. Hancock *et al.*, "Free-space propagation of spatiotemporal optical vortices," *Optica*, vol. 6, no. 12, pp. 1547–1553, Dec. 2019, doi: 10.1364/OPTICA.6.001547.

[21] A. Chong, C. Wan, J. Chen, and Q. W. Zhan, "Generation of spatiotemporal optical vortices with controllable transverse orbital angular momentum," *Nature Photon.*, vol. 14, pp. 350–324, Feb. 2020, doi: 10.1038/s41566-020-0587-z.

[22] Z. R. Mei, O. Korotkova, and E. Shchepakina, "Electromagnetic multi-Gaussian Schell-model beams," *J. Opt.*, vol. 15, no. 2, Feb. 2013, Art. no. 025705, doi: 10.1088/2040-8978/15/2/025705.

[23] X. D. Chen and D. M. Zhao, "Propagation properties of electromagnetic rectangular multi-Gaussian Schell-model beams in oceanic turbulence," *Opt. Commun.*, vol. 372, pp. 137–143, Aug. 2016, doi: 10.1016/j.optcom.2016.03.082.

[24] Z. S. Tong and O. Korotkova, "Electromagnetic nonuniformly correlated beams," *J. Opt. Soc. Amer. A*, vol. 29, no. 10, pp. 2154–2158, Oct. 2012, doi: 10.1364/JOSAA.29.002154.

[25] C. L. Ding *et al.*, "Propagation properties of stochastic electromagnetic non-uniformly correlated partially coherent pulses in dispersive media," *J. Opt.*, vol. 15, no. 10, Oct. 2013, Art. no. 105707, doi: 10.1088/2040-8978/15/10/105707.

[26] Y. J. Cai, Y. H. Chen, and F. Wang, "Generation and propagation of partially coherent beams with nonconventional correlation functions: A review," *J. Opt. Soc. Amer. A*, vol. 31, no. 9, pp. 2083–2096, Sep. 2014, doi: 10.1364/JOSAA.31.002083.

[27] Z. R. Mei and O. Korotkova, "Electromagnetic cosine-Gaussian Schell-model beams in free space and atmospheric turbulence," *Opt. Exp.*, vol. 21, no. 22, pp. 27246–27259, Nov. 2013, doi: 10.1364/OE.21.027246.

[28] Y. J. Li, "Laguerre-Gaussian functions and generalized formulation of electromagnetic Gaussian Schell-model sources," *J. Opt. Soc. Amer. A*, vol. 32, no. 5, pp. 877–885, May 2015, doi: 10.1364/JOSAA.32.000877.

[29] M. L. Luo and D. M. Zhao, "Twisted anisotropic electromagnetic beams with Laguerre Gaussian-Schell model correlation," *Opt. Exp.*, vol. 28, no. 21, pp. 31360–27259, Oct. 2020, doi: 10.1364/OE.401670.

[30] C. L. Ding, O. Korotkova, Y. T. Zhang, and L. Z. Pan, "Cosine-Gaussian correlated Schell-model pulsed beams," *Opt. Exp.*, vol. 22, no. 1, pp. 931–942, Jan. 2014, doi: 10.1364/OE.22.000931.

[31] P. Paakkonen, J. Turunen, P. Vahimaa, A. T. Friberg, and F. Wyrowski, "Partially coherent Gaussian pulses," *Opt. Commun.*, vol. 204, no. 1-6, pp. 53–58, Apr. 2002, doi: 10.1016/S0030-4018(02)01240-3.

[32] Q. Lin, L. G. Wang, and S. Y. Zhu, "Partially coherent light pulse and its propagation," *Opt. Commun.*, vol. 219, no. 1–6, pp. 65–70, Apr. 2003, doi: 10.1016/S0030-4018(03)01340-3.

[33] H. Lajunen, P. Vahimaa, and J. Tervo, "Theory of spatially and spectrally partially coherent pulses," *J. Opt. Soc. Amer. A*, vol. 22, no. 8, pp. 1536–1545, Aug. 2005, doi: 10.1364/JOSAA.22.001536.

[34] F. Q. Kong *et al.*, "Generating few-cycle radially polarized pulses," *Optica*, vol. 6, no. 2, pp. 160–164, Jan. 2019, doi: 10.1364/OPTICA.6.000160.

[35] Y. Li and M. Gao, "Turbulence-induced changes in the state of polarization of partially polarized, partially coherent pulsed electromagnetic beams propagating through anisotropic turbulence," *Opt. Eng.*, vol. 58, no. 11, Nov. 2019, Art. no. 116107, doi: 10.1117/1.OE.58.11.116107.

[36] Y. Li *et al.*, "Anisotropic turbulence-induced statistical properties evolution of a radially polarized partially coherent pulsed beam on propagation," *Opt. Commun.*, vol. 466, Jul. 2020, Art. no. 125669, doi: 10.1016/j.optcom.2020.125669.

[37] Y. Li and M. Gao, "Spectral and coherent properties of partially polarized pulsed electromagnetic beams upon turbulent atmosphere propagation for different source conditions," *Appl. Phys. B*, vol. 126, pp. 34, Feb. 2020, doi: 10.1007/s00340-020-7380-z.

[38] F. Gori, V. R. Sanchez, M. Santarsiero, and T. Shirai, "On genuine cross-spectral density matrices," *J. Opt. A Pure Appl. Opt.*, vol. 11, no. 8, May 2009, Art. no. 085706, doi: 10.1088/1464-4258/11/8/085706.

[39] H. Roychowdhury and O. Korotkova, "Realizability conditions for electromagnetic Gaussian Schell-model sources," *Opt. Commun.*, vol. 249, no. 4–6, pp. 379–385, May 2005, doi: 10.1016/j.optcom.2005.01.054.

[40] S. J. Zhu *et al.*, "Generation and propagation of a vector cosine-Gaussian correlated beam with radial polarization," *Opt. Exp.*, vol. 23, no. 26, pp. 33099–33115, Dec. 2015, doi: 10.1364/OE.23.033099.

[41] T. Voipio, T. Setala, and A. T. Friberg, "Coherent-mode representation of partially polarized pulsed electromagnetic beams," *J. Opt. Soc. Amer. A*, vol. 30, no. 11, pp. 2433–2443, Nov. 2013, doi: 10.1364/JOSAA.30.002433.

[42] J. P. Zhang *et al.*, "Propagation characteristics of a twisted cosine-Gaussian correlated radially polarized beam," *Appl. Sci.*, vol. 8, no. 9, pp. 1485, Aug. 2018, doi: 10.3390/app8091485.